Biomedicine & Pharmacotherapy 188 (2025) 118204

Contents lists available at ScienceDirect

Biomedicine & Pharmacotherapy

journal homepage: www.elsevier.com/locate/biopha

Hericium erinaceus extracts promote neuronal differentiation and excitability through nootropic metabolite activity

Federico Brandalise [a], Erica Cecilia Priori [b], Francesca Giammello [b,c], MariaTeresa Venuti [b], Daniela Ratto [b], Lorenzo Goppa [d,e], Carlo Alessandro Locatelli [f], Elena Savino [d], Elisa Roda [f], Paola Rossi [b,*]

[a] Department of Biomedical Sciences, Division of Neuroscience and Clinical Pharmacology, University of Cagliari, Cittadella Universitaria di Monserrato, Monserrato 09042, Italy
[b] Department of Biology and Biotechnology "L. Spallanzani", University of Pavia, Pavia 27100, Italy
[c] PhD Program in Genetics, Molecular and Cellular Biology, University of Pavia, Italy
[d] Department of Earth and Environmental Sciences (DSTA), University of Pavia, Pavia 27100, Italy
[e] PhD Program in Earth and Environmental Sciences, University of Pavia, Italy
[f] Laboratory of Clinical & Experimental Toxicology, Pavia Poison Centre, National Toxicology Information Centre, Toxicology Unit, Istituti Clinici Scientifici Maugeri IRCCS Pavia, Pavia 27100, Italy

ARTICLE INFO

Keywords:
Neuroblastoma
SH-SY5Y
Hericium erinaceus
Neuronal differentiation
Patch clamp
Voltage-gated sodium currents
Cell proliferation
Action potential
Erinacines
Hericenones
Voltage-Gated Sodium Channel

ABSTRACT

This study investigates the effects of a blend of *Hericium erinaceus* (lion's mane mushroom) extract on the differentiation of SH-SY5Y cells, a human neuroblastoma cell line, revealing potential therapeutic implications for neuroblastoma management. Treatment with this blend induced cells differentiation towards a neuron-like profile, as evidenced by enhanced neuronal excitability and upregulation of neuronal markers, such as βIII-tubulin and synaptotagmin. Additionally, the treatment significantly reduced PCNA, a key regulator of proliferation, alongside a decrease in stemness markers, indicating a shift toward a more mature and less proliferative phenotype. These findings demonstrate the ability of *Hericium erinaceus* to promote neuronal differentiation and inhibit proliferation in neuroblastoma cells, highlighting its therapeutic potential for managing neuroblastoma and potentially other neurological disorders. The results suggest that *Hericium erinaceus* may serve as a promising candidate for the development of novel neuroregenerative therapies.

1. Introduction

Neuroblastoma stands as one of the most aggressive pediatric cancers, posing a challenge in oncology due to its complex etiology and variable clinical manifestations[1]. Originating from neural crest progenitor cells, it primarily affects young children and displays a spectrum of behaviors, from spontaneous regression to aggressive metastasis[2]. Despite advances in surgery, chemotherapy, and radiotherapy, the prognosis for high-risk neuroblastoma remains poor (5-year relative survival rate ~50 %)[3], highlighting the urgent need for novel therapeutic strategies.

The SH-SY5Y cell line is widely used as a model in neuroblastoma research, offering a tractable system to study the disease's molecular mechanisms and therapeutic responses[4]. These cells retain several tumor-like features and can differentiate into neuronal-like cells upon exposure to various factors, reflecting neurogenesis processes [1–3].

Various protocols have been employed to induce differentiation in SH-SY5Y cells, encompassing a diverse range of inducers and methodologies. For instance, retinoic acid, a derivative of vitamin A, has been extensively utilized to drive neuronal differentiation in SH-SY5Y cells by activating retinoic acid receptors and downstream signaling pathways involved in neurogenesis [4]. Similarly,

Abbreviations: TPA 12-O, tetradecanoylphorbol-13-acetate; He, *Hericium erinaceus*; MTT assay 3, 4,5-dimethylthiazol-2-yl-2,5-diphenyltetrazolium bromide assay; Cm, Membrane capacitance; Rm, Membrane resistance; Vm, Resting membrane potential; TTX, Tetrodotoxin; VGSC, Voltage-gated sodium channel; I-V plots, Current-voltage plots; SNARE, Soluble N-ethylmaleimide-sensitive factor Attachment protein REceptor; PCNA, Proliferating Cell Nuclear Antigen.

* Corresponding author.
E-mail address: paola.rossi@unipv.it (P. Rossi).

https://doi.org/10.1016/j.biopha.2025.118204
Received 15 January 2025; Received in revised form 19 May 2025; Accepted 21 May 2025
Available online 24 May 2025

12-O-tetradecanoylphorbol-13-acetate (TPA), a potent protein kinase C activator, has been shown to induce neuronal differentiation in SH-SY5Y cells by modulating intracellular signaling cascades [5]. Additionally, brain-derived neurotrophic factor (BDNF), a neurotrophin crucial for neuronal survival and differentiation, has been employed to promote neuronal differentiation in SH-SY5Y cells, highlighting the diverse array of strategies available to researchers for studying neuronal differentiation in this cell model [6,7].

Recently, natural compounds have emerged as promising tools in neuroprotection and neuroregeneration[1 2-1 3]. Among these, *Hericium erinaceus* (H. erinaceus), also known as lion's mane mushroom, has attracted attention for its neurotrophic properties. Its extracts contain bioactive compounds such as erinacines and hericenones, which have been shown to stimulate BDNF and nerve growth factor (NGF) production[1 4-1 7], key regulators of neuronal survival, differentiation, and synaptic plasticity.

Recent publications, such as the studies conducted by Mori et al. and Brandalise et al. have significantly contributed to our understanding of the neuroregenerative properties inherent in H. erinaceus extract [8–10]. These investigations, along with others [11,12], have elucidated the extract's remarkable capacity to not only enhance neurogenesis but also to ameliorate cognitive decline in animal models of neurodegenerative diseases. Kawagishi et al. [13] uncovered compelling evidence about the extract's ability to stimulate neurogenesis, a process crucial for brain repair and cognitive function in human astrocytoma cells. Similarly, Rossi et al., 2018's study underscored the extract's potential in mitigating cognitive decline [11], thereby highlighting its promise as a therapeutic agent for neurodegenerative disorders.

Building on this background, we hypothesize that long-term exposure to H. erinaceus extract promotes neuronal differentiation in SH-SY5Y cells. Through extended treatment, we aim to evaluate its potential to reduce proliferative activity and support differentiation, offering a novel perspective on neuroblastoma intervention.

2. Materials and methods

2.1. Cells and treatments

2.1.1. SH-SY5Y cells

SH-SY5Y cells, a human neuroblastoma cell line provided by ATCC (ATCC CRL- 2266) (Manassas, Virginia, US), were grown in a 1:1 mix of DMEM and Ham's F12 supplemented with 10 % FBS and 1 % penicillin/streptomycin at 37 °C and 5 % CO_2. When reaching confluence, cells were divided and plated in a new fresh growth medium. Cell passaging was performed by centrifugation at 1900 rpm for 7 minutes before resuspension in the new fresh growth medium. Cells were always maintained at low passages (between 3 and 10). All cell culture reagents were purchased from Euroclone (Milan, Italy). Complete culture medium was supplemented with 50 μg/mL He1 + 50ug/mL He2. The treatment for H. erinaceus (He) condition was performed by plating and maintaining cells in He1 + He2 supplemented culture medium for > 200 hours, with a maximum of 288 hours. To ensure the maintenance of nutrients in the cell culture throughout the entire duration of the treatment, cells were plated at low confluence with 25 % more medium compared to standard growth conditions, and the essential parameters for cell cultivation (cell culture media volume and pH) were monitored daily.

2.1.2. LUHMES cells

LUHMES cells (Lund Human Mesencephalic; originally derived from human female fetal mesencephalon; ATCC, VA, USA) were cultured and differentiated following established protocols [14,15]. Cells were maintained at 37 °C in a humidified incubator with 5 % CO_2. For proliferation, LUHMES cells were grown in Advanced DMEM/F-12 (Thermo Fisher Scientific, Waltham, MA, USA), supplemented with 2 mM L-glutamine (Thermo Fisher), 1 × N2 supplement (Thermo Fisher), and 40 ng/mL basic fibroblast growth factor (bFGF, PeproTech). Flasks or plates were pre-coated with poly-L-ornithine (50 μg/mL, Sigma-Aldrich) and fibronectin (1 μg/mL, Sigma-Aldrich). For differentiation, cells were plated at a density of 2–4 × 10^4 cells/cm^2 in differentiation medium consisting of Advanced DMEM/F-12 supplemented with 1 × N2, 2 mM L-glutamine, 1 mM dibutyryl cyclic AMP (Sigma-Aldrich), 2 ng/mL glial cell line-derived neurotrophic factor (GDNF, PeproTech), and 1 μg/mL tetracycline (Sigma-Aldrich). Media was refreshed every other day. Differentiation was carried out for 10 days to allow maturation into post-mitotic dopaminergic-like neurons. For electrophysiological recordings, cells were plated on 12 mm glass coverslips pre-coated with poly-L-ornithine (10 μg/mL) and laminin (10 μg/mL, Sigma-Aldrich). After the 10-day differentiation period, LUHMES cells were treated with the He blend at the same concentration used for SH-SY5Y cells (50 μg/mL He1 + 50 μg/mL He2) and for an equivalent duration (>200 hours) to ensure experimental consistency across cell models

2.1.3. Preparation of Mushroom Extracts

Two strains of He collected in Italy has been used in this work, He1 and He2. The mycelia of these strains were isolated in pure culture from sporophores collected in a Mediterranean environment from living oaks (Siena province, Tuscany, Italy). The strains were identified by molecular analysis and preserved in MicUNIPV, the Fungal Research Culture Collection at the University of Pavia (Italy) [16]. In particular, He1 mycelium and He2 cultivated sporophore were chosen. The procedures for extracting compounds from these strains have been thoroughly documented in several studies [24–26]. For the alcoholic extraction, 1 g of both lyophilized He1 mycelium (obtained from liquid culture containing 2 % Malt extract) and He2 sporophore cultivated at the Botanical Garden greenhouse (Pavia University, Italy) was blended with 10 mL of ethanol 70 % and 30 % water, left in the thermostat at 50 °C for 24 h. At the end, the material was transferred for centrifugation (4000 rpm for 3 min) and the supernatant was stored at −20 °C for HPLC analysis [17–19]. The metabolites were identified and measured through HPLC-UV-ESI/MS analyses, previously described [24–26]. This method allows for the precise identification and quantification of various metabolites present in the extract. Specific standards and carefully calibrated curves were utilized to ensure the accuracy and reliability of the measurements. Standard compounds of erinacines and hericenones were kindly provided by Prof. Hirokazu Kawagishi (Shizuoka University, Japan), as previously reported [18], while ergothioneine was kindly donated by Tetrahedron (Paris, France). The erinacine A content in He1 mycelium (150 μg/g) is consistent with those reported by Krzyczkowski et al. (2010) in enhanced submerged cultivation studies [18]. He2 sporophore contains high levels of hericenones C (1560 μg/g) and D (188 μg/g). Ergothioneine was present in both the He1 mycelium (0.58 mg/g) and in He2 sporophore (2.4 mg/g), giving a final ergothioneine concentration of 2.98 mg/g. These values align with the findings for certain strains reported by Lee et al. (2016) [19]. The erinacine A content in He1 mycelium (150 μg/g) is consistent with those reported by Krzyczkowski et al. (2010) [20]. He2 sporophore contains high levels of hericenones C (1560 μg/g) and D (188 μg/g). Ergothioneine was present in both the He1 mycelium (0.58 mg/g) and in He2 sporophore (2.4 mg/g), giving a final ergothioneine concentration of 2.98 mg/g. These values align with the findings for certain strains reported by Lee et al. (2016) [21].

2.1.4. MTT assay

In order to select the appropriate, non-toxic He dose to be used in the following analyses, as a first experimental step, a range of He mixture concentration was evaluated through the MTT [3-(4,5-dimethylthiazol-2-yl)-2,5-diphenyltetrazolium bromide]. Briefly, SH-SY5Y cells were seeded in a 96-well plate at a density of 10,000 cells/well (0.2 mL medium per well) and incubated for 24 hours in a humidified atmosphere containing 5 % of CO_2. The following day, the culture medium was replaced with fresh medium added with He1 and He2 in combination in

a concentration ranging from 5 to 250 µg/mL. For the control condition, cells were incubated with the culture medium only. After 48 h-exposure, 20 µL of MTT solution (HelloBio, UK) was added to each well; this operation was performed in the dark, and the plates were subsequently incubated for 3 hours at 37°C. Cell viability was then assessed by measuring the samples' absorbance at 550 nm using the Multiplate reader BioTek ELx808 (Italy). As a background value, all experiments were conducted while assessing in parallel blank samples containing He1, He2 and MTT in culture medium (without cells) to exclude the occurrence of non-enzymatic reduction of MTT by He1 and He2. The optical density of the formazan formed in the control group cells was taken as 100 %. Cell viability % was calculated as follows:

$$\text{Cell viability\%} = \frac{(\text{Absorbance value of treated cells} - \text{Absorbance value of blank})}{(\text{Absorbance value of untreated cells} - \text{Absorbance value of blank})} \times 100.$$

2.1.5. Patch-Clamp Experiments

Electrical signals were recorded with an Axopatch 200-B amplifier (Molecular Devices, USA), [−3 dB; cutoff frequency (fc) = 1 kHz] and sampled with a Digidata-1440A interface. Electrophysiological recordings were performed in Whole-Cell configuration on SH-SY5Y cells. Cells were recorded in a bath solution containing (in mM): NaCl 130, KCl 4, Hepes 10, glucose 10, $CaCl_2$ 2, $MgSO_4$ 1, pH 7.4. Glass borosilicate pipettes were pulled using Flaming/Brown micropipette puller P-97 (Sutter Instrument Co., USA) to achieve a 4–7 MΩ resistance and were filled with (in mM): K^+- gluconate 126, NaCl 4, Hepes 5, glucose 15, $MgSO_4$ 1, BAPTA FREE 0,1, BAPTA Ca^{2+} 0005, ATP 3. GTP 0,1 pH 7.2. The current recordings in voltage clamp configuration were performed with the following protocols: a series of voltage steps ranging from −60 mV to + 140 mV with an increment of 20 mV, and a series of voltage steps ranging from −120 mV to + 40 mV with an increment of 20 mV at a sampling rate of 20 kHz were delivered to the cells. The passive properties of the cell (including membrane resistance and capacitance) were measured by eliciting a hyperpolarizing step of −10 mV from the holding potential of −60 mV [22,23].

For the depolarizing protocols, the PN leak subtraction of the Clampex program (pClamp 10 software) was used to eliminate the effects of the leakage current on the whole-cell responses [24,25]. The following compounds were bath-perfused in the patch-clamp experiments: TTX 1 µM (Hello Bio), Nifedipine 10 µM (Hello Bio), to selectively block the VGSC-mediated current [26]. Current-clamp recordings: The resting membrane potential (RMP) was assessed after break in the cell. The holding potential was set according to a value ~-70 mV. The current clamp protocol consisted of a series of 5 pA steps of current injection, starting from a negative injection of −10 pA. Outward currents were measured in voltage clamp by applying subsequent voltage steps of + 20 mV from a holding potential of −60 mV, up to + 140 mV [27]. Steady outward currents were recorded as the average of the last 50 ms of the voltage step. Inactivating outward currents were calculated by subtracting the sustained outward current from peak outward currents [28]. Inward currents were calculated in voltage clamp as the negative peak recorded at 0 mV by applying subsequent voltage steps of + 20 mV from a holding potential of −120 mV, up to + 40 mV [29]. Electrophysiological analysis and statistics were performed using Clampfit 10.6 (Molecular Devices), OriginPro 9.1 and GraphPad Prism version 10.0.0 for Windows.

2.1.6. Phase contrast microscopy

SH-SY5Y cells were plated on 22 × 22 mm coverslip at a density of 10.000 cells per coverslip and observed under inverted phase contrast microscopy equipped with a 20 × objective (Olympus CKX41) after 24, 72, 144 and 200 hours exposure to He (50µl/mL + 50µl/mL) with the aim to evaluate the onset of potential changes/alteration of cell morphology. Digital micrographs were acquired with a camera (Olympus MagniFire digital camera), stored on a PC and processed with the Olympus CellˆF 3.1 software. The analysis of cell density was performed using ImageJ software 1.54 (NIH, USA). Specifically, four random images in each well were acquired at 40 × magnification for each replicate and then converted to binary images and analyzed with the "particle analysis tool". The cell density was calculated as number of cells/area and expressed in mm [2]. Data are presented as the mean ± SEM. The number and the length of neurite were analyzed by the semi-automated tracing ImageJ plugin NeuronJ. Using this plugin, neurites are manually traced, thanks to an algorithm that compares the pixel intensity on the neurite with its adjacent pixel neighborhoods, automatically updating the cursor to follow an estimated path of the neurite and increasing the accuracy and speed of tracing. After the neurites are traced, a text file is generated that contains measurements of the lengths of all the neurites [30].

2.1.7. Hematoxylin and eosin and Nissl staining

For the morphological evaluations, control and treated cells were grown on coverslips (22 mm×22 mm), fixed with 4 % formalin (20 min), and post-fixed with 70 % ethanol at −20°C for at least 24 h. The samples were rehydrated for 10 min in PBS 1X and then were incubated with hematoxylin and eosin or Nissl stainings. For Hematoxylin and eosin, the samples were incubated with hematoxylin for 10 minutes, washed with PBS 1x, and stained with eosin for 30 seconds. For Nissl, the slides were incubated with cresyl violet 0.1 % for 5 minutes. Lastly, for both staining, cells were washed in PBS 1X and mounted with a drop of Mowiol (Calbiochem-Inalco, Italy) for microscopy visualization.

2.1.8. Clonogenic assay

Cells were plated in a 6 well plate at a density of 300 cells/well in 2 mL of control and He supplemented growth medium. Cells were then incubated at 37 °C for a minimum of 10 days, to allow optimal growth of the colonies. After 11 days cells were fixed using ice-cold methanol and colonies were colored with Crystal Violet (CV) 0,1 % (PanReac AppliChem, Italy) to evaluate the number and area of colonies obtained in different conditions. Digital micrographs were acquired with a camera (Olympus MagniFire digital camera), stored on a PC and processed with the Olympus CellˆF software (version n. 3.1). The analysis of cell density was performed using ImageJ software 1.54 (NIH, USA). Specifically, four random images in each well were acquired at 20 × magnification for each replicate and then converted to binary images and analyzed with the "particle analysis tool". The cell area was expressed in mm [2]. Data are presented as the mean ± SEM.

2.1.9. Immunofluorescence Reactions

For the immunofluorescence quantifications, three independent experiments were performed for each experimental condition. After reactions, control and treated cells were grown on coverslips (22 mm×22 mm), fixed with 4 % formalin (20 min), and post-fixed with 70 % ethanol at −20°C for at least 24 h. The samples were rehydrated for 10 min in PBS and then incubated with 1 % Bovine Serum Albumin (BSA) to block nonspecific binding sites. Subsequently, the cells were immunolabeled using the mouse monoclonal anti-bIII tubulin (ValidAb, Hello Bio, UK), the mouse monoclonal anti-PCNA (Merck, Italy), the rabbit monoclonal antibody anti-CD133 (Cell Signaling Technology,

USA), the mouse polyclonal antibody anti-Nav (Neuromab, USA), the rabbit polyclonal antibody anti-Synaptotagmin-1,2 (Abcam, Cambridge, UK), diluted 1:200, 1:200, 1:200, 1:250, 1:200 in PBS (Merck, Italy) for 1 hour at RT in a dark, moist chamber. Then, the cells were washed with PBS and incubated for 45 min with goat anti-mouse IgG (H + L) highly cross-adsorbed secondary antibody, Alexa Fluor Plus 594 and goat anti-mouse IgG (H + L) highly cross-adsorbed secondary antibody, Alexa Fluor Plus 488 both diluted 1:200 in PBS (Thermo Fisher Scientific, Italy), and phalloidin conjugated with Alexa Fluor 488. DNA counterstaining was performed using 0.1 mg/mL Hoechst 33258 (Merck, Italy). Lastly, cells were mounted with a drop of Mowiol (Calbiochem-Inalco, Italy) for microscopy visualization.

2.1.10. Immunocytochemical Evaluations

For the immunofluorescence quantifications, three independent experiments were performed for each experimental condition. After reactions, coverslips were examined using a Leica DM6B WF microscope (Leica microsystems, Italy), and images were captured with an ORCA-Flash4.0 V3 Digital CMOS camera C13440–20CU (Hamamatsu Photonics, Italy), and results were analyzed using the Leica Application Suite X (LAS X) software (Version 5.1.0). For each condition, 11 quadrants (about 50 cells) were evaluated for random analysis. Single-channel images were analyzed in grayscale, with the minimum value being 0 (black) and the maximum value being 255 (white). The mean fluorescence intensity was measured using ImageJ software 1.54 (NIH, USA) and expressed as the mean ± SEM.

To prevent potential discrepancies in results caused by slight procedural variations, all immunostaining reactions were simultaneously performed, and, as a control, some cells were incubated without primary antibodies, using only PBS; any immunoreactivity was observed under this condition. To assess the immunopositivity of cells for the examined markers, all experiments were conducted in parallel with bank samples incubated without primary antibodies. In detail, the mean fluorescence intensity of blank samples was subtracted from the mean fluorescence intensity of immunostained cells. Immunopositivity was established when the mean fluorescence intensity value of single cells exceeded that of the blank samples.

2.2. Statistical analysis

All data are expressed as the mean ± standard error of the mean (SEM) based on the experimental values obtained from three independent experiments conducted under identical conditions. Statistical significance was determined at three levels: $p < 0.05$ (*), $p < 0.01$ (**), and $p < 0.001$ (***). For comparisons between two groups, the Mann-Whitney *U* test or unpaired *t*-test was applied, depending on the distribution and variance of the data. For multiple group comparisons, one-way or two-way analysis of variance (ANOVA) was performed to evaluate the interaction effects of independent variables. When significant differences were identified, post hoc tests, including Bonferroni's test or Dunnett's test, were conducted to pinpoint specific group differences while controlling for multiple comparisons. The analyses were performed using Prism software (GraphPad, version X) and Origin 2021 (OriginLab), with all statistical methods validated for appropriate assumptions regarding data normality and variance. Prior to parametric testing, data distribution was assessed using the Shapiro-Wilk test, and homogeneity of variances was verified using Levene's test. Nonparametric tests were employed when data failed to meet these assumptions.

2.3. Development of a standardized Hericium erinaceus blend: harnessing synergistic bioactive properties

Before evaluating the effects of *Hericium erinaceus* (He) extracts on SH-SY5Y cells, assessed in terms of morphological, molecular and physiological changes, we firstly determined the optimal blend to be tested. Hence, after a comprehensive analysis of various strains of He from the Italian peninsula at our disposal, we selected two distinct extracts, namely He1 and He2, which we have previously characterized [19,20,28–30]. Based on these knowledge, we proposed a blend composed of He1 and He2, with the clear notion in mind that it can provide a wide array of nootropic bioactive metabolites, in high concentrations (for details, see Table 1).

Table 1
Concentration of selected nootropic bioactive metabolites in the blend (He1 + He2). Values are expressed as micrograms per gram of dried extract (μg/g).

Bioactive Metabolites	Quantity (μg per gram of dried extract)
Erinacine A	150
Hericenones C	1560
Hericenones D	188
Ergothioneine	2980

Among these compounds, Erinacine A is recognized for its neuroprotective properties [31–33], while Ergothioneine serves as a potent antioxidant [34–36]. Conversely, Hericenones C and D have demonstrated significant neurotrophic and anti-inflammatory effects [13]. Hence, based on He1 and He2 complementary bioactive profile, we selected sporophore extract and mycelium extract for He2 and He1, respectively. By blending these latter in a 1:1 ratio, we aim at harnessing a comprehensive spectrum of He nootropic metabolites, potentially offering synergistic benefits for neuronal health, leveraging the distinct but complementary properties of each extract. Such a blend may enhance cellular resilience against oxidative stress, promote neuronal growth, and mitigate inflammatory responses, thereby providing a multifaceted defense against neurodegenerative processes.

3. Results

3.1. Establishment of optimal concentration of Hericium erinaceus extracts

The SH-SY5Y cell line has emerged as a well-known model for neuronal differentiation [1], hence this in vitro model was chosen to test the effects/properties of the blend, made by mycelium of He1 and sporophore of He2. For convenience, the blend will be referred to as "He" from this point on in the manuscript. As the initial step in our experimental procedure, we identified the appropriate He concentration to be tested. Therefore, an MTT assay was performed to assess cell viability following 72 hours exposure to increasing concentrations of He (Fig. 1a). The combined exposure to 50 μg/mL He1 and 50 μg/mL He2 results in a viability reduction of 1.60 ± 4.22 % (n = 3) (Fig. 1a). Therefore, the blend containing 50 μg/mL of He1 and 50 μg/mL of He2 extracts was selected for the following experiments (see Methods).

3.2. Morphological changes and reduced proliferation in He-exposed SH-SY5Y cells

Based on previous studies revealing that He extracts are capable to influence cell morphology and proliferation rates, we initially focused on these aspects to understand He effects on SH-SY5Y cells. Specifically, we investigated the morphological changes of SH-SY5Y cells in response to He treatment. Literature data well documented that when SH-SY5Y cells are induced to differentiate using agents such as TPA, they adopt a more elongated, neurite-bearing phenotype resembling mature neurons [37]. Additionally, neurotrophic factors like BDNF have been shown to promote neuronal differentiation and reduce proliferation in SH-SY5Y cells by activating specific signaling pathways [38].

To characterize cellular morphology and to assess potential differentiation phenomena, hematoxylin and eosin (H&E) and Nissl staining were performed (Fig. 1b) after 200 hours of He 50ug/mL exposure. The staining revealed noticeable differences in cell morphology comparing control and He-treated cells. In fact, control cells appeared closely

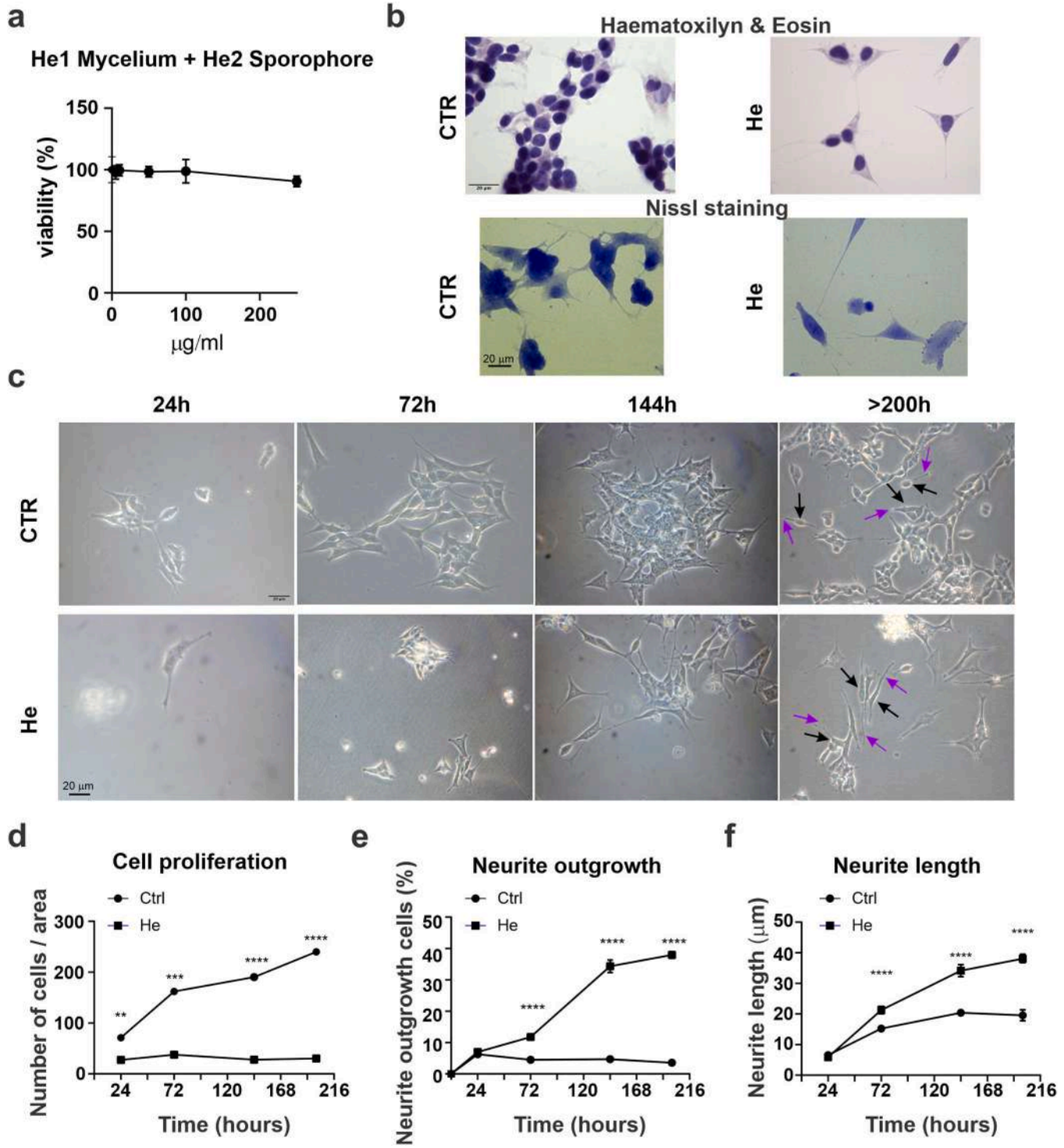

Fig. 1. Time-dependent reduction of cell proliferation and enhancement of neurite outgrowth in SH-SY5Y cells following He exposure, rich in nootropic bioactive metabolites. (a) Cell viability assessment: SH-SY5Y cells were treated with increasing concentrations (0, 5, 10, 50, 100, 250 µg/mL) of a blend combining He mycelium (He1) and sporophore (He2) extracts. Cell viability (% relative to untreated control) was measured. (b) Hematoxylin and eosin staining: micrographs displaying cellular morphology of SH-SY5Y cells under control (CTR) and He-treated conditions (He). Scale bar: 20 µm. (c) Representative phase-contrast images: morphological changes and neurite extension in SH-SY5Y cells under CTR conditions and after 24, 72, 144, and over 200 hours exposure to He. Black arrows point to the cell body of the cells while purple arrow indicate the location of some neurites (d) Quantification of cell proliferation: number of cells per area (148 µm2) at selected time points for both CTR and He-treated groups. (e) Neurite outgrowth analysis: percentage of cells exhibiting neurite outgrowth over time in CTR and He-treated groups. (f) Neurite length measurement: average neurite length at various time points, highlighting significant elongation in the He-treated group.

packed with less pronounced cytoplasmic extensions, whereas He-treated cells exhibited elongated cell bodies and extended neurites, suggestive of neuronal differentiation.

To have a better resolution of these morphological changes while simultaneously tracking the proliferation rate, we employed phase-contrast microscopy to observe neurite outgrowth, a hallmark of

neuronal differentiation, both in control and He-treated condition (Fig. 1c). This approach allowed us to monitor dynamic cellular processes and provided a more detailed comprehension of He-induced differentiation.

Cell proliferation analysis was conducted at different time points to determine the effect of He treatment on cells growth rate (Fig. 1c). Data revealed a significant decrease in cell proliferation comparing He-treated cells with the control group, already 24 hours after exposure, further exacerbated at prolonged exposure times (number of cells/area; 24 h: CTR 85.00 ± 2.88, n = 3; He 28.66 ± 0.88, n = 3; $p = 4.8 \times 10^{-5}$,

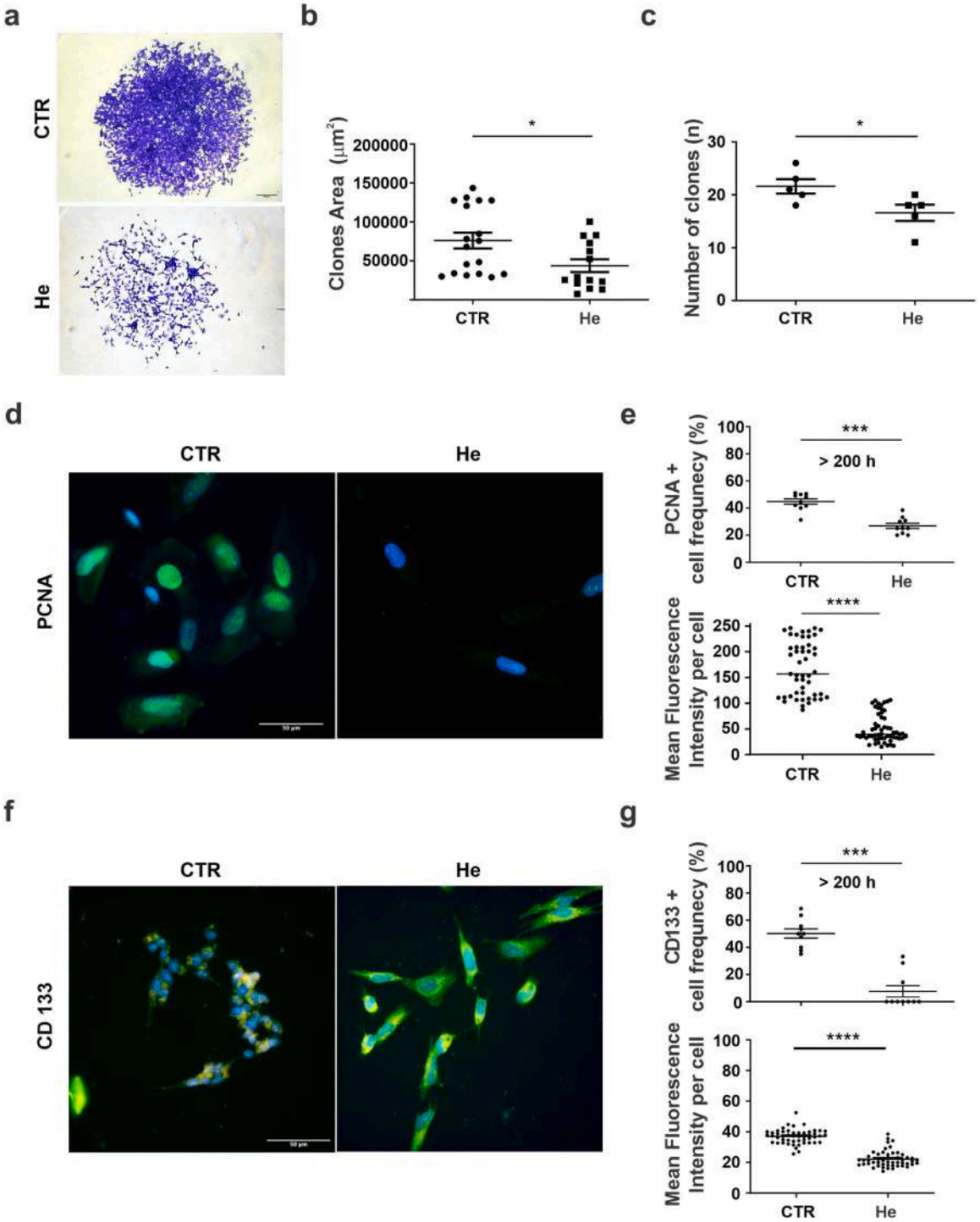

Fig. 2. Effects of He Treatment on Colony Forming, Proliferation and Stemness marker expression (a) Colony forming assay: representative micrographs of crystal violet-stained colonies showing noticeable morphological differences comparing control (CTR) and He-treated SH-SY5Y cells. (b) Quantitative analysis of colony area. (c) Quantitative analysis of the number of colonies. (d) Representative immunofluorescence images of PCNA staining in SH-SY5Y cells under control conditions (CTR) and after > 200 hours exposure to He. PCNA immunolabelling: green fluorescence; DNA (stained with Hoechst 33258): blue fluorescence. Scale bar: 50 μm. (e) Quantitative analysis of PCNA: immunopositive cell frequency (%) and mean fluorescence intensity per cell in control and He-treated groups. (f) Representative immunofluorescence images of CD133 staining in SH-SY5Y cells in control conditions (CTR) and after > 200 hours He exposure. CD133 immunolabelling: green fluorescence; DNA (stained with Hoechst 33258): blue fluorescence. Scale bar: 50 μm. (g) Quantitative analysis of CD133: immunopositive cell frequency (%) and mean fluorescence intensity per cell in control and He-treated groups.

unpaired *t*-test; 72 h: CTR 170.00 ± 4.16, n = 3; He 39.66 ± 2.03, n = 3; p = 9.5 × 10^{-6}, unpaired *t*-test; 144 h: CTR 190.16 ± 0.84, n = 3; He 27.94 ± 2.22, n = 3; p = 2.75 × 10^{-6}, unpaired *t*-test; >200 h: CTR 240.0 ± 3.96, n = 3; He 30.26 ± 1.59, n = 3; p = 1.02 × 10^{-6}, unpaired *t*-test, Fig. 1d). Morphological analysis indicated a significant increase in neurite outgrowth over time in He-treated cells compared to control group starting from 72 hours (% of cell with neurite; 24 h: CTR 4.716 ± 0.16, n = 3; He 6.99 ± 0.22, n = 3; p = 0.001, unpaired *t*-test; 72 h: CTR 4.51 ± 0.201, n = 3; He 11.75 ± 0.41, n = 3; p = 9.1 × 10^{-5}, unpaired *t*-test; 144 h: CTR 4.67 ± 0.15, n = 3; He 34.32 ± 2.02, n = 3; p = 1.26 × 10^{-4}, unpaired *t*-test; >200 h: CTR 3.57 ± 0.19, n = 3; He 37.94 ± 1.04, n = 3; p = 5.36 × 10^{-7}, unpaired *t*-test; Fig. 1e). Consistently, the measurement of neurite length revealed a significant increase in He-treated cells compared to control starting at 72 hours (CTR: ~15.00 ± 1.50 μm; He: ~25.00 ± 1.80 μm), at 144 hours (CTR: ~19.00 ± 1.70 μm; He: ~38.00 ± 1.60 μm), and at 200 hours (CTR: 19.55 ± 1.79 μm, n = 48; He: 38.08 ± 1.48 μm, n = 48; p < 0.0001, ANOVA followed by Šidák's multiple comparisons test, Fig. 1f).

3.3. He Treatment reduces clonogenic capability, proliferation and stemness marker expression

In the previous chapter, we demonstrated that the proliferation rate of SH-SY5Y cells is decreased in the presence of He, accompanied by elongated neurites. These characteristics are typically associated with reduced stemness and enhanced differentiation. To investigate the effects of He on SH-SY5Y cell proliferation and differentiation, we performed colony formation assays parallelly assessing key proliferation and stemness markers. The colony forming assays revealed a significant reduction both in colony area and colony number in He-treated cells compared to the control group (Fig. 2a). Quantitative analysis showed that the colony area was significantly reduced in the He-treated cells (CTR: 76,089 ± 10,106 μm^2, n = 18; He: 43,797 ± 8265 μm^2, n = 14; p = 0.0242, unpaired *t*-test; Fig. 2b). Similarly, the number of colonies formed by He-treated cells was markedly diminished compared to control group (CTR: 21.60 ± 1.36, n = 5; He: 16.60 ± 1.53, n = 5; p = 0.0409, unpaired *t*-test; Fig. 2c). These findings suggest that He treatment reduces the clonogenic capability of SH-SY5Y cells, indicating a potential shift towards a more differentiated state.

To further evaluate this shift, we analyzed the expression of PCNA (Proliferating Cell Nuclear Antigen) and CD133, as typical markers associated with proliferation and stemness, respectively. Immunofluorescence staining revealed a notable reduction in PCNA expression in He-treated cells compared to controls (Fig. 2d). Quantitative evaluation indicated a significant decrease both in the frequency of PCNA-immunopositive cells (CTR: 67.85 ± 4.19 %, n = 6; He: 27.48 ± 4.19 %, n = 6; p = 0.0002, unpaired *t*-test, Fig. 2e top) as well as in the mean fluorescence intensity per cell (CTR: 95.46 ± 11.38, n = 6; He: 40.91 ± 11.38, n = 6; p = 0.0007, unpaired *t*-test; Fig. 2e bottom). These results indicate that He exposure significantly suppresses cell proliferation. Additionally, the assessment of CD133 expression showed a significant reduction in He-treated cells compared to controls (Fig. 2f). The frequency of the CD133-immunoreactive cells substantially decreased in the He-treated group (CTR: 71.00 ± 3.08 %, n = 6; He: 35.50 ± 3.08 %, n = 6; p = 0.0002, unpaired *t*-test, Fig. 2g top). Likewise, the mean fluorescence intensity per cell was significantly lower in He-treated group (CTR: 36.94 ± 0.67, n = 50; He: 22.15 ± 0.75, n = 50; p < 0.0001, unpaired *t*-test; Fig. 2g bottom). This reduction in CD133 expression further supports the idea that He treatment promotes differentiation towards a more mature neuronal phenotype.

Collectively, these results indicate that He treatment significantly suppresses proliferation and promotes differentiation in SH-SY5Y cells. The reduced colony formation, paralleled by the decreased PCNA and CD133 expression, corroborate the hypothesis that He is capable to induce a shift towards a differentiated neuronal state.

3.4. Passive properties analysis of SH-SY5Y cells after prolonged exposure to he

Previous studies have shown that He have an impact neuronal cells and oligodendrocytes, by modulating their morphology and functional properties [8,28,39,40]. Specifically, He has been reported to induce changes in cell morphology, such as neurite outgrowth and myelin production. Given these reported effects, we hypothesized that the morphological changes induced by He could also impact their passive electrophysiological properties. Changes in cell morphology, such as neurite elongation, are known to influence parameters like input resistance, membrane time constant, and capacitance, which are crucial for cellular excitability and signalin. To investigate this, we sought to measure the electriophysiological passive membrane properties of our *in vitro* model. Specifically, using patch-clamp recordings, we examined the cells passive properties such as Membrane Capacitance (Cm) and Membrane Resistance (Rm) to assess any alterations induced by He treatment, comparing the control group with the one receiving a prolonged exposure (> 200 hours) to He (Fig. 3a). While the fast component of the membrane time constant (t_{fast}) was unchanged in the two conditions (CTR: 0.19 ± 0.03 ms, n = 16; He: 0.18 ± 0.03 ms, n = 14; p = 0.59, Mann-Whitney Test, Fig. 3b left) the slow component of the membrane time constant (t_{slow}) was significantly slower in He group compared to the control one (CTR: 0.60 ± 0.09 ms, n = 17; He: 14.92 ± 0.16 ms, n = 14; p = 0.018, Mann-Whitney Test, Fig. 3b right).

Likewise, a significant increment in Cm was detected in He -treated SH-SY5Y cells (CTR: 10.91 ± 1.31 pF, n = 17; He: 14.92 ± 1.34 pF, n = 19; p = 0.04, Mann-Whitney Test, Fig. 3c left). Instead, no differences were observed between the control and He group for the Rm (CTR: 1.02 ± 0.11 GΩ, n = 16; He: 1.00 ± 0.10 GΩ, n = 18; p = 0.81, Mann-Whitney Test, Fig. 3c center) and the resting membrane potential (Vm) (CTR: −35.63 ± 2.32 mV, n = 16; He: −32.53 ± 2.24 mV, n = 17; p = 0.30, Mann-Whitney Test, Fig. 3c right). Overall, these findings indicate that He treatment modulates the slow component of the membrane time constant and the membrane capacitance, consistently with the observed increase in neurite outgrowth and so cellular surface of the distal compartment. These electrophysiological changes likely reflect underlying mechanisms of neuronal differentiation and functional maturation following prolonged exposure to He.

3.5. He treatment induces electrophysiological changes in inward and outward currents of SH-SY5Y cells

Inward currents play a crucial role in neuronal differentiation and maturation, with their expression and magnitude influencing the developmental state of neurons [41–44]. To investigate the effects of He treatment on these currents, we examined the kinetic properties of inward currents in SH-SY5Y cells (Fig. 4a). Our analysis revealed notable differences between control and He-treated cells. Although the time to peak was similar between the two groups (CTR: 46.14 ± 1.1 ms, n = 13; He: 43.25 ± 0.95 ms, n = 15; p = 0.065, Mann-Whitney Test; Fig. 4b), He-treated cells exhibited significantly shorter half-width (CTR: 3.34 ± 0.48 ms, n = 14; He: 2.13 ± 0.35 ms, n = 15; p = 0.0064, Mann-Whitney Test; Fig. 4b), rise time 10–90 % (CTR: 1.97 ± 0.48 ms, n = 15; He: 0.86 ± 0.09 ms, n = 14; p = 0.0073, Mann-Whitney Test; Fig. 4b), and decay time (CTR: 6.81 ± 1.56 ms, n = 13; He: 3.12 ± 0.33 ms, n = 15; p = 0.0307, Mann-Whitney Test; Fig. 4b). These findings suggest that He treatment positively modulates the kinetic of inward currents, consistent with an increase in Nav-mediated currents, which are typically characterized by faster activation and inactivation compared to Cav-mediated currents. To further elucidate the mechanisms underlying these changes, we compared the current-voltage (I-V) relationships of inward currents between control and He-treated cells. The I-V plots revealed that the peak current amplitude occurred at similar holding potentials for both groups (~0 mV). This observation remained consistent regardless of whether we analyzed absolute peak

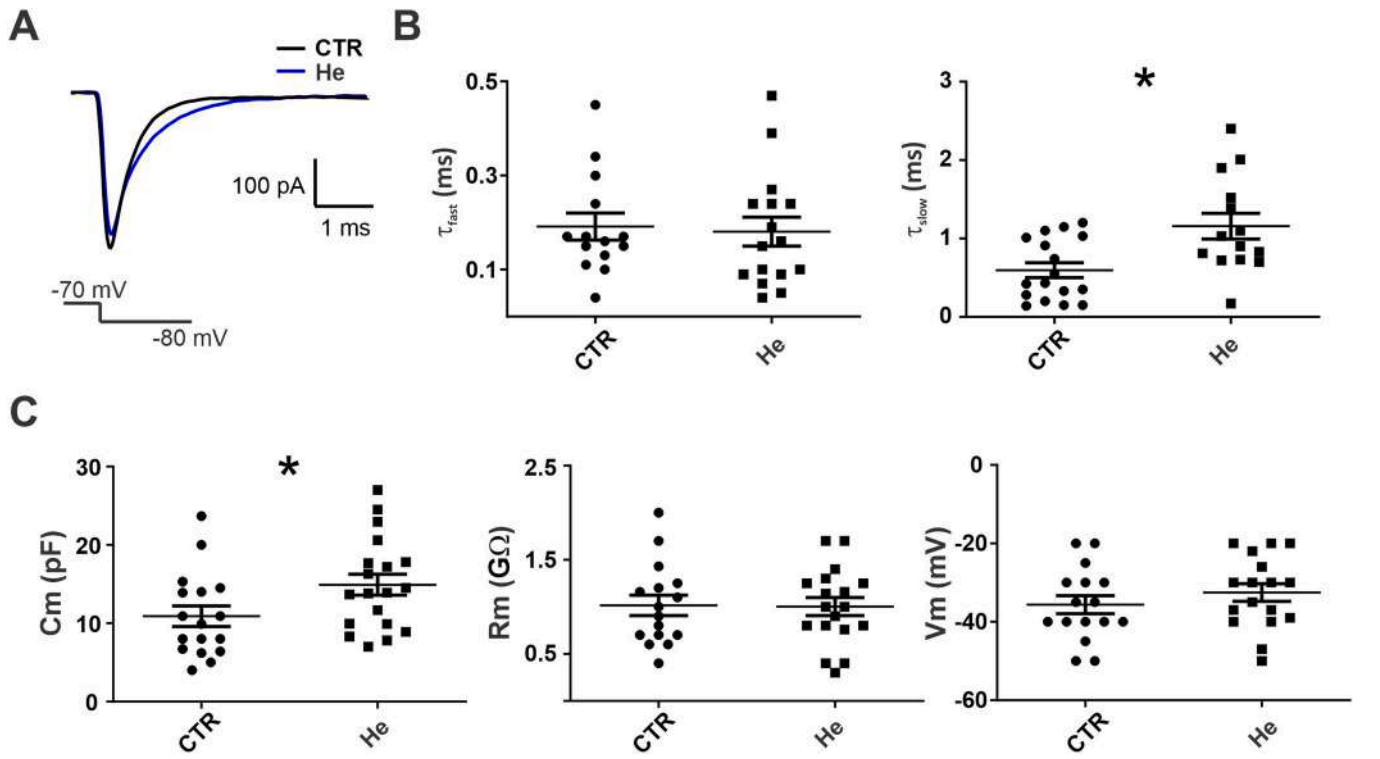

Fig. 3. Passive properties analysis of the SH-SY5Y cells reveals higher membrane capacitance and unchanged membrane resistance and resting membrane potential after > 200 hours of He compared to the control condition (CTR). (a) Representative averaged traces from control (black) and > 200 hours of He exposure (blue), showing the response to a hyperpolarizing voltage step from −80 mV to −70 mV. (b) Pool data for all of the recorded cells for Membrane Time Constant Fast and Slow (τ fast, τ slow), and (c) membrane capacitance (Cm), membrane resistance(Rm) and resting membrane potential (Vm).

amplitudes or normalized the values to the maximum current (Fig. 4c,d). These results indicate that the He-induced upregulation of inward currents is primarily due to an increase in channel density rather than a shift in activation properties.

Outward currents are also critical for neuronal differentiation and the development of action potentials. To assess the impact of He treatment on outward potassium currents, we analyzed steady-state outward currents in SH-SY5Y cells subjected to incremental depolarizing steps from a holding potential of −60 mV. This protocol was specifically designed to minimize contamination from inward current components. We observed a significant reduction in the outward steady-state current in the He-treated group compared to controls. The control group exhibited a peak outward current amplitude of 887.3 ± 380.4 pA (n = 12), whereas He-treated cells showed a markedly lower amplitude (381.8 ± 248.2 pA; n = 14; p = 0.0003, Mann-Whitney Test, Fig. 4f). Additionally, analysis of the distribution of cells with steady-state and inactivating outward currents revealed a significant shift in He-treated cells. Specifically, 42.9 % of He-treated cells exhibited inactivating outward currents, whereas no such expression was detected in control cells (Fig. 4g). These findings suggest that He treatment alters potassium channel expression or function, which may contribute to the observed changes in the electrophysiological profile of SH-SY5Y cells.

Together, these results demonstrate that He treatment induces substantial changes in both inward and outward currents, influencing the kinetic properties of Nav and Cav channels, as well as the amplitude and type of potassium currents. These electrophysiological changes likely reflect underlying mechanisms of neuronal differentiation and functional maturation following prolonged exposure to He extract.

3.6. Long-term exposure to he increases Na+ TTX-sensitive currents

We investigated the effects of long-time He treatment on the functional development of voltage-dependent currents in SH-SY5Y cells. SH-SY5Y cells displayed a variety of inward and outward currents under both control (CTR) and He-treated conditions. Incremental depolarizing voltage-clamp steps were applied to analyze inward currents. He-treated cells showed a significant increase in inward current amplitude compared to controls (CTR: −342.8 ± 34.98 pA, n = 12; He: −737 ± 122.1 pA, n = 13; p = 0.004, Mann-Whitney test, Fig. 5a, b). To assess the contribution of voltage-gated sodium channels (Nav) to these inward currents, we applied tetrodotoxin (TTX, 1 μM), a selective Nav blocker. TTX significantly reduced inward currents in both groups (CTR baseline: −392.80 ± 79.45 pA; CTR TTX: −238.60 ± 40.95 pA; p = 0.0098, paired *t*-test; He baseline: −640.20 ± 214.10 pA; He TTX: −4.00 ± 4.00 pA; p = 0.0418, paired *t*-test, Fig. 5a, c). The percentage reduction of TTX-sensitive current was significantly greater in He-treated cells (CTR: 38.6 ± 3.5 %, n = 5; He: 99.00 ± 1 %, n = 5; p = 0.0079, Mann-Whitney test, Fig. 5c). To investigate the temporal dynamics of inward current modulation, we performed a time-course analysis over a 216-hour period (Fig. 5d). At baseline (0 h), the mean inward current peak amplitude was –317.5 ± 54.5 pA in control cells (n = 4) and –188.8 ± 25.2 pA in He-treated cells (n = 4). While the current amplitude remained relatively stable in the control group, reaching –380.0 ± 58.3 pA at 216 hours (n = 5), He-treated cells exhibited a progressive and marked increase in inward current amplitude, reaching –621.4 ± 119.5 pA at 216 hours (n = 7). This difference between groups was statistically significant (p = 0.0025, Mann–Whitney test). To explore the residual TTX-insensitive current, we applied nifedipine (5 μM), a blocker of L-type calcium channels (Cav). Nifedipine significantly reduced inward current in control cells (CTR baseline: −282.6 ± 71.16 pA; CTR nifedipine: −84.40 ± 23.28 pA; p = 0.0357, paired *t*-test, Fig. 5e, f), but had no significant effect in He-treated cells (He baseline: −322.4 ± 91.44 pA; He nifedipine: −296.2 ± 76.48 pA; p = 0.2007, paired *t*-test, Fig. 5e, f). The percentage reduction was significantly higher in control cells (CTR: 66.34 ± 7.8 %, n = 5; He: 5.92 ± 2.73 %, n = 5; p = 0.0159, Mann-Whitney test, Fig. 5f). These results indicate that He treatment

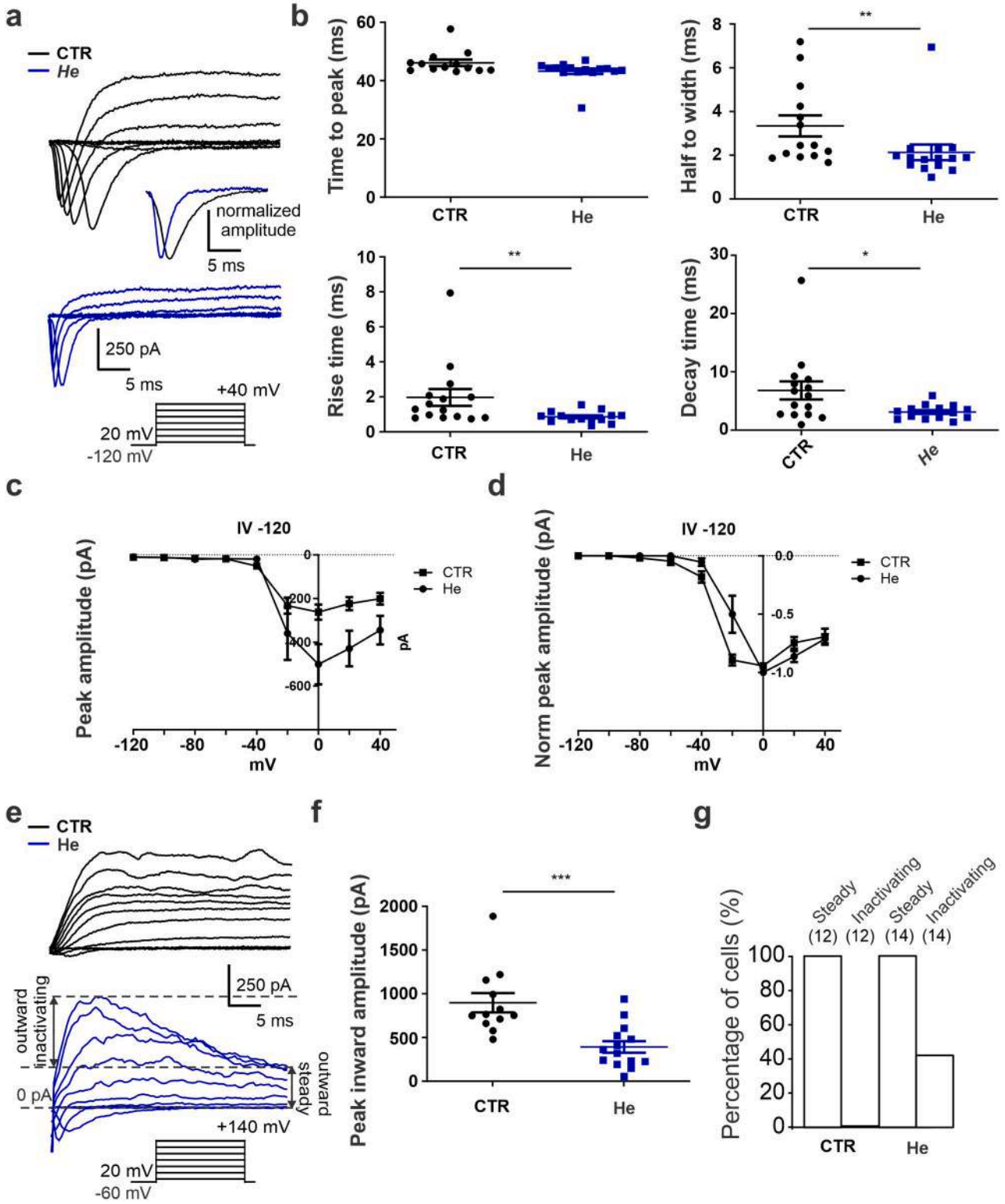

Fig. 4. Differential Impact of He on Inward and Outward Conductances Density. a) Example traces of inward and outward currents repertoire from control (black) and He treated cells (blue) in response to depolarizing voltage steps from −120 mV to + 40 mV. Inset: Schematic of the voltage protocol and amplitude normalization of the inward current from a representative example of a record derived from the control and He condition. (b) Quantification of kinetic properties of inward currents in control and treated groups: time to peak (top left), half-width (top right), rise time (bottom left), and decay time (bottom right). (c) Average I-V plot showing peak inward current amplitude as a function of voltage for control and Hericium treated cells. d) Normalized peak inward current amplitude for control and treated cells, normalized to the maximum amplitude for each group. (e) Example traces from control (black) and He treated cells (blue) for progressively depolarized voltage steps from −60 mV to + 140 mV, showing the inactivating and steady-state outward currents. (f) Pooled data showing peak outward current amplitude for control and treated cells. (g) Percentage of cells displaying steady-state and inactivating outward current profiles for both control and He-treated groups.

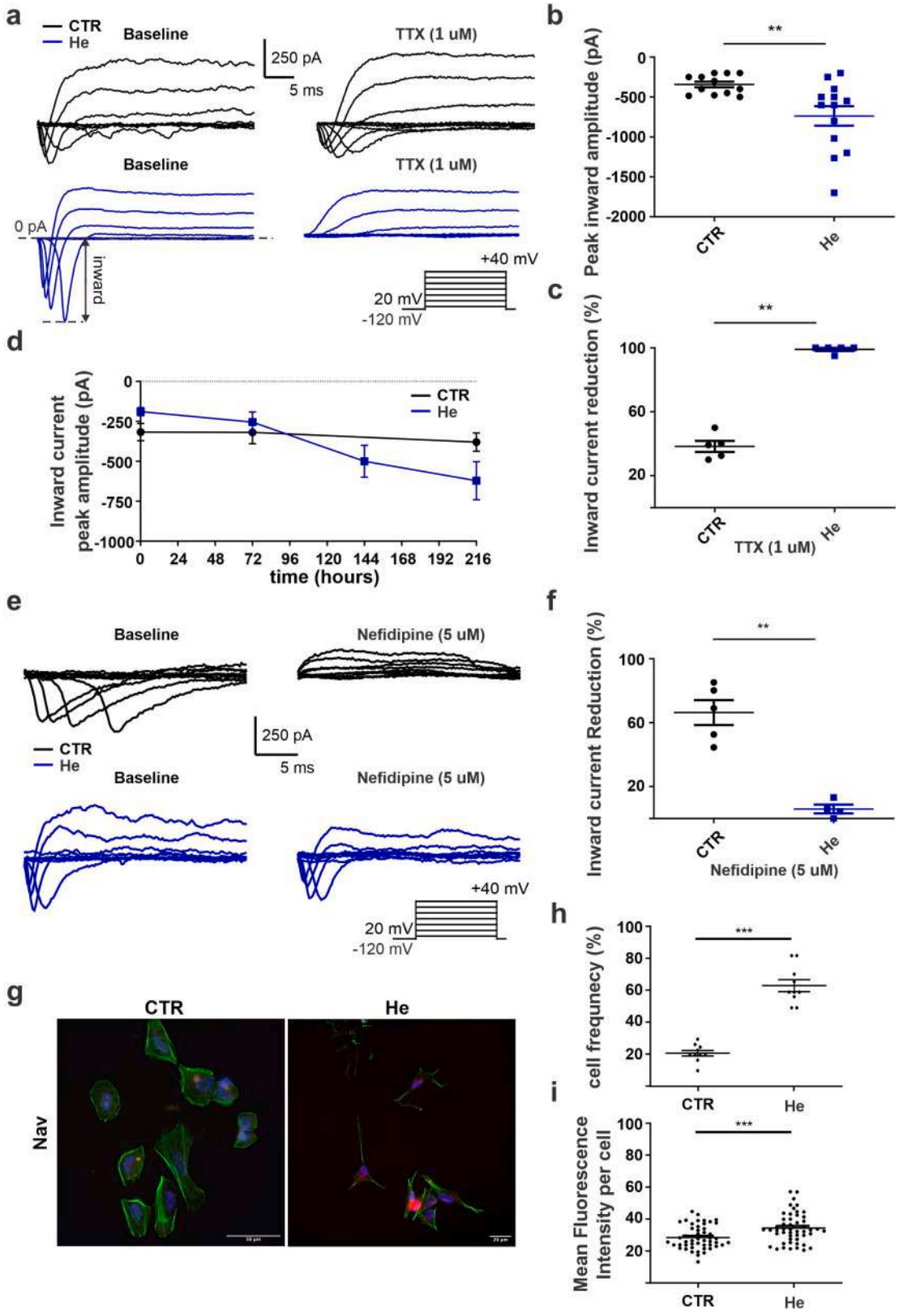

Fig. 5. Electrophysiological and Immunofluorescence Analyses of SH-SY5Y Cells After He Treatment. (a) Representative traces of inward current recordings from SH-SY5Y cells in control (black) and after > 200 hours of He treatment (blue), showing responses to depolarizing voltage steps from −120 mV to + 40 mV at baseline and after TTX (1 μM) application. (b) Summary plot of peak inward current amplitudes for control and He-treated groups. (c) Percentage reduction in inward current amplitude following TTX application for control and He-treated cells. (d) Time-course analysis of peak inward current amplitude in control and He-treated cells over 216 hours (e) Representative traces of inward currents in control (black) and He-treated cells (blue) before and after Nifedipine (5 μM) application. (f) Percentage reduction in inward current amplitude following Nifedipine application for control and He-treated cells.

leads to a dominance of TTX-sensitive currents (Nav) and a reduction in Cav activity. Immunofluorescence analysis showed that He-treated cells had higher Nav channel expression compared to controls (Fig. 5g). Quantitative analysis revealed a significant increase in the frequency of Nav-positive cells (CTR: 25.00 ± 4.8 %, n = 8; He: 67.50 ± 3.5 %, n = 8; $p < 0.001$, unpaired *t*-test, Fig. 5h). Additionally, the mean fluorescence intensity per cell was significantly higher in He-treated cells (CTR: 28.49 ± 1.051, n = 49; He: 34.39 ± 1.321, n = 50; $p < 0.001$, unpaired *t*-test, Fig. 5i).

These findings demonstrate that long-term exposure to He enhances the expression and function of Nav channels in SH-SY5Y cells, while reducing the contribution of Cav channels. This shift in ion channel activity may underlie the electrophysiological changes associated with He-induced neuronal differentiation.

3.7. Enhanced neuronal excitability and marker expression following he treatment

Nav channels are primarily expressed in excitable cells and play a critical role in initiating action potentials (APs). Given the observed increase in Nav channel expression, we hypothesized that He treatment might enhance cell excitability, resulting in a more pronounced action potential profile. This hypothesis aligns with existing literature suggesting that differentiated SH-SY5Y cells exhibit increased action potential firing. To assess this, current-clamp experiments were conducted on SH-SY5Y cells both under control and He-treated conditions. Depolarizing current steps of increasing amplitude were injected into the recorded cells, and changes in membrane potential along with AP frequency were recorded (Fig. 6a). The analysis revealed that a higher proportion of He-treated cells displayed single APs compared to control cells, where a notable subset failed to produce APs in response to current injection (CTR single AP: 60.8 %, n = 14/23; CTR no AP: 34.9 %, n = 8/23; He single AP: 78 %, n = 14/18; He no AP: 0 %, n = 0/18; Fig. 6b). Moreover, a significant fraction of He-treated cells exhibited repetitive AP firing (CTR repeated AP: 4.3 %, n = 1/23; He repeated AP: 22 %, n = 4/18; Fig. 6b), resembling neuronal activity patterns.

The latency to the first AP against the injected current, showed results between the two groups (Fig. 6c) and the AP frequency plotted against the injected current indicated that He-treated cells achieved a maximum firing frequency of 24.8 ± 9.7 Hz (n = 3, Fig. 6d), resembling to some cortical [45], hippocampal excitatory cells [46] and amygdala neuron [22]. Analysis of AP characteristics demonstrated a significant increase in AP amplitude in He-treated cells (CTR: 33.18 ± 5.59 mV, n = 8; He: 52.86 ± 4.63 mV, n = 7; $p = 0.03$, Mann-Whitney test, Fig. 6e). Additionally, AP duration was significantly shorter in He-treated cells (CTR: 38.44 ± 11.41 ms, n = 8; He: 23.95 ± 11.65 ms, n = 9; $p = 0.0254$, Mann-Whitney test, Fig. 6f), and the AP threshold was more depolarized (CTR: −53.13 ± 1.67 mV, n = 8; He: −45.56 ± 2.69 mV, n = 9; $p = 0.046$, Mann-Whitney test, Fig. 6g).

These findings suggest that He treatment enhances the excitability of SH-SY5Y cells, likely due to increased functional expression of Nav channels, thereby enhancing AP characteristics and differentiation toward a neuronal-like phenotype.

To corroborate the differentiation induced by He treatment, we evaluated the expression of neuronal markers, specifically βIII-tubulin and synaptotagmin, which are indicative of neuronal differentiation and synaptic vesicle release, respectively (Fig. 6h,k). Immunofluorescence evaluation, assessed both in terms of immunopositive cell frequency and optical density (OD), revealed that βIII-tubulin immunoreactivity was significantly higher in He group (βIII-tubulin: CTR: 40.5 % ± 5.8, n = 10/23; He: 72.2 % ± 4.5, n = 13/18; $p < 0.001$, unpaired *t*-test, Fig. 6h,i) which also showed a significantly higher βIII-tubulin expression, as indicated by OD (>200 hours CTR: 34.66 ± 3.69 A.U., n = 37; >200 hours He: 72.26 ± 6.81 A.U., n = 37; $p = 0.00039$, unpaired *t*-test, Fig. 6h,j). Similarly, synaptotagmin-immunopositive cells frequency was significantly higher in the He group (synaptotagmin: CTR: 10 % ± 3.5, n = 1/10; He: 65 % ± 6.8, n = 6/10; $p < 0.0001$, unpaired *t*-test, Fig. 6k,l). Synaptotagmin expression, associated with the SNARE complex and neurotransmitter release, was also significantly elevated in He-treated cells (>200 hours CTR: 29.87 ± 1.28 A.U., n = 10; He: 67.50 ± 10.86 A.U., n = 10; $p < 0.0001$, unpaired *t*-test, Fig. 6k,m). These results support the hypothesis that prolonged He exposure promotes SH-SY5Y cell differentiation toward a neuronal-like state, paralleled by reduced proliferative capacity. To assess whether the differentiation effects observed with the He blend could be attributed to a single compound, we exposed SH-SY5Y cells to Ergothioneine (ERGO) alone for > 200 hours at the same concentration present in the blend (2.98 mg/g). While no significant changes were detected in action potential (AP) properties such as amplitude, duration, or threshold, a higher proportion of cells were able to elicit a single AP compared to the control group (Supplementary Fig. 1). The absence of more robust electrophysiological changes and repetitive firing, however, indicates that ERGO alone is insufficient to reproduce the full neuronal phenotype. Consequently, these findings support the conclusion that the complete He metabolite spectrum, with its nootropic properties, is required to achieve the full extent of neuronal differentiation and functional maturation previously described. To strengthen the physiological relevance of our findings and address concerns about appropriate controls, we additionally tested the effect of the He extract on LUHMES cells differentiated into dopaminergic-like neurons. In this model, He treatment did not significantly alter resting membrane potential, rheobase, or spontaneous firing frequency, suggesting the extract does not interfere with the basal electrophysiological properties of healthy neuronal cells (Supplementary Fig. 2).

4. Discussion

In the present study, we demonstrate that treatment with He extract for approximately 200 hours induces a pronounced shift towards a neuron-like phenotype in SH-SY5Y cells, a well-established human neuroblastoma cell line commonly utilized as an in vitro model for studying neurodevelopmental processes and evaluating potential therapeutic interventions. This neurogenic effect is characterized by enhanced voltage-gated sodium current and expression of neuronal markers such as βIII-tubulin and reduction in markers linked to cell proliferation such as PCNA, corroborating the differentiation process.

Medicinal mushrooms have been increasingly recognized for their potential anticancer properties, as highlighted in several recent reviews [47–49]. These fungi, particularly those used in traditional Chinese medicine, contain a plethora of bioactive compounds such as polysaccharides, lectins, and triterpenoids, which exhibit a variety of antitumor activities [50].

Another significant aspect of He's anticancer activity is its ability to inhibit angiogenesis [51]. By blocking angiogenesis, He effectively starves the tumor, preventing its growth and spread. Studies have identified that the erinacines [52] and hericenones in He can inhibit angiogenesis, highlighting their potential in anti-tumor strategies.

Moreover, He has been found to possess immunomodulatory properties, enhancing the body's immune response against cancer cells [53]. Polysaccharides from this mushroom stimulate the activity of macrophages, natural killer cells, and lymphocytes, which are crucial for detecting and destroying malignant cells. This immunostimulatory effect not only aids in direct tumor suppression but also enhances the effectiveness of other cancer treatments [54].

Clinical studies and animal models further support the anticancer potential of He. For instance, in models of colon cancer, extracts from He has been shown to reduce tumor size and inhibit metastasis [55]. Additionally, in vitro studies on human gastric cancer cells have demonstrated that He extracts can suppress cell proliferation and induce apoptosis [56].

He has garnered attention for its remarkable pro-neuronal properties, underpinned by its rich composition of bioactive compounds [33,

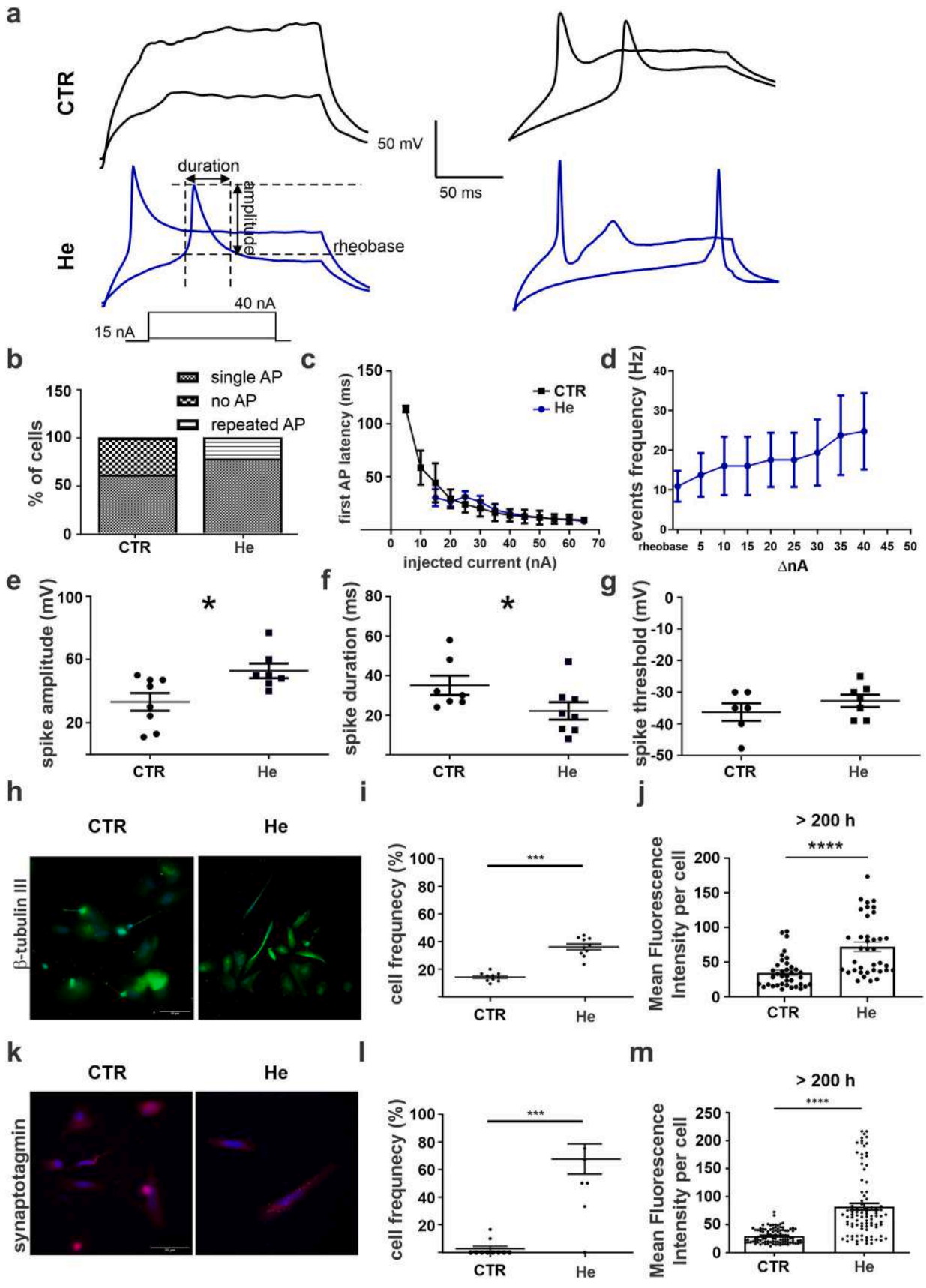

(caption on next page)

Fig. 6. SH-SY5Y cells treated with He exhibit increased excitability and expression of neuronal markers compared to the control group. a) Representative action potential (AP) traces recorded in current clamp mode from SH-SY5Y cells in the control group (black, CTR) and the He-treated group (blue, He) in response to the same current injection (15–40 nA). Parameters measured include AP amplitude, duration, threshold, and rheobase. (b) Percentage of cells responding to the current injection protocol with no AP, single AP, or repeated firing of APs in both conditions (CTR vs. He). (c) Comparison of the latency to the first AP as a function of injected current between CTR and He-treated cells. (d) Frequency of events (Hz) in He-treated cells as a function of incremental current steps (ΔnA). (e) Quantification of AP amplitude (mV) showing significant differences between CTR and He groups. (f) Quantification of AP duration (ms), revealing a significant reduction in He-treated cells compared to CTR. (g) Comparison of AP threshold (mV) between CTR and He cells. (h) Representative micrographs showing immunofluorescence labelling for βIII-tubulin in CTR and He-treated cells. (i) βIII-tubulin-immunopositive cell frequency (%) in both groups, demonstrating a significant increase in He-treated cells. (j) βIII-tubulin mean fluorescence intensity per cell, revealing a marked upregulation in He group after > 200 hours exposure. k) Representative micrographs depicting immunofluorescence labelling for synaptotagmin in CTR and He-treated cells. (l) Synaptotagmin-immunopositive cell frequency (%) showing significantly higher levels in He group. (m) Synaptotagmin mean fluorescence intensity per cell in CTR and He groups after > 200 hours exposure, indicating a significant increase in the expression of synaptic marker after He treatment.

57]. These compounds, including polysaccharides and hericenones, have been extensively studied for their ability to promote neuronal survival, neurite outgrowth, and synaptic plasticity [58,59]. Brandalise et al. demonstrated the pro-neuronal potential of He extract in a study where treatment with the extract led to enhanced synaptic pruning in hippocampal rat organotypic slice cultures [28]. Similarly, Mori et al. conducted a clinical trial in elderly individuals with mild cognitive impairment, showing significant improvements in cognitive function following supplementation with He extract [60]. These findings underscore the promising role of in promoting neurogenesis and neuronal function, offering potential therapeutic perspective for neurological disorders.

Our study adds relevant insights to the growing body of publications supporting the differentiation-inducing effects of He extract. Mori et al. provided insights into the underlying mechanisms, demonstrating the nerve growth factor (NGF)-inducing activity of He in human astrocytoma cells [8]. NGF plays a crucial role in promoting neuronal differentiation and survival, making it a key mediator of He-induced differentiation. The bioactive compounds in He, particularly erinacines and hericenones, are most likely responsible for mimicking NGF activity or enhancing NGF production, as evidenced by studies demonstrating their ability to stimulate NGF synthesis in astrocytes and promote neuronal differentiation [8,13,33]. In cancer biology, inducing differentiation is a recognized strategy to impede cancer progression, as differentiated cancer cells typically exhibit reduced proliferative rates and increased susceptibility to therapeutic interventions. The differentiation-inducing potential of He extract offers a promising avenue for combating neuroblastoma and other neurodevelopmental disorders.

While various differentiation protocols already exist, such as those utilizing retinoic acid and TPA, their clinical translation is hindered by several limitations. Retinoic acid, for example, is known to exhibit teratogenic effects and has poor blood-brain barrier permeability, limiting its therapeutic utility in neurological disorders. TPA, on the other hand, is associated with cytotoxicity and inflammation, posing safety concerns for long-term use. In contrast, He extract is well-tolerated and capable of crossing the blood-brain barrier, making it an attractive candidate for therapeutic interventions. Furthermore, its differentiation-inducing effects offer a safer and more efficacious alternative to existing protocols, potentially overcoming the translational barriers associated with conventional agents. Voltage-gated ion channels play a pivotal role in neuronal differentiation and maturation, with their expression and activity dynamically regulated during development.

Voltage-gated calcium channels (VGCCs) are crucial for mediating calcium influx, which drives processes such as neurotransmitter release, gene expression, and neurite outgrowth. However, their expression tends to decrease as neurons mature, reflecting a shift in ion channel functionality during differentiation. For instance, high-voltage-activated calcium currents decrease during cerebellar granule cell development in situ [43,44], while inwardly rectifying potassium currents and VGSC expression patterns emerge distinctively during differentiation [43]. These changes underscore the critical shift from voltage gated calcium channel towards voltage dependent sodium channel supporting the functional maturation of neurons.

In the context of He treatment, our findings suggest that He modulates this ion channel remodeling process. Specifically, He treatment leads to a significant upregulation of VGSC-mediated inward currents, accompanied by a reduction in VGCC activity. This shift may reflect an advanced differentiation and maturation state induced by He, aligning with its observed ability to promote neuronal marker expression and suppress proliferation.

The observed effects of He extract on neurite outgrowth and inward current amplitude upregulation suggest a multifaceted mechanism of action. The rapid onset of these effects, evident within 24 hours of application, implies the involvement of fast-acting signaling pathways, such as possibly the NGF-TrkA pathway. NGF, a key neurotrophic factor, plays a pivotal role in promoting neurite outgrowth and synaptic plasticity, suggesting its potential involvement in mediating He-induced differentiation [13,33,58]. Additionally, the progressive enhancement of these effects over 200 hours suggests a more profound influence, potentially involving modulation of gene expression. This prolonged effect may entail the activation of transcription factors and epigenetic modifiers, leading to sustained changes in neuronal phenotype and function. Further elucidation of these mechanisms is essential for understanding the therapeutic potential of He extract and its implications for neuroblastoma management. In conclusion, our study demonstrates that He extract promotes neuronal differentiation and reduces proliferation in SH-SY5Y neuroblastoma cells. The observed shift toward a neuron-like phenotype, characterized by increased expression of neuronal markers and enhanced voltage-gated sodium currents highlights the extract's potential as a differentiation-inducing agent. Given the known blood–brain barrier permeability of HE extract [61] and its pronounced *in vitro* effects on neuronal differentiation, further *in vivo* studies are currently being planned to evaluate its efficacy in neuroblastoma models. These investigations will also explore potential synergistic effects with existing therapies and assess the safety profile of prolonged exposure.

Author contributions

FG, ECP, FB, performed the experiments. FG, ECP, FB, CL, PR analyzed the data, participated in language editing and manuscript revision. FG, ECP, FB, MV, DR, LG contributed to the *in vitro* experiments. PR, FB, ER, ES conceived and designed the study. ER, PR and FB provided the conception and design of the study, PR, ES, ER, FB participated in the drafting and revision and supervised the study. All authors contributed to the article and approved the submitted version.

CRediT authorship contribution statement

Daniela Ratto: Writing – review & editing, Supervision, Methodology. **MariaTeresa Venuti:** Software, Methodology, Data curation. **Carlo Alessandro Locatelli:** Validation, Conceptualization. **Lorenzo Goppa:** Visualization, Investigation. **Elisa Roda:** Resources, Methodology, Data curation. **Elena Savino:** Writing – review & editing,

Validation, Supervision. **Paola Rossi:** Writing – review & editing, Writing – original draft, Visualization, Validation, Supervision, Funding acquisition, Formal analysis, Data curation, Conceptualization. **Erica Cecilia Priori:** Writing – original draft, Investigation, Formal analysis. **Federico Brandalise:** Writing – review & editing, Writing – original draft, Investigation, Formal analysis, Data curation, Conceptualization. **Francesca Giammello:** Writing – original draft, Investigation, Formal analysis.

Funding

This research was funded by (i) the University of Pavia, Fondi Ricerca Giovani (FRG 2020), Department of Biology and Biotechnology "L. Spallanzani", University of Pavia and (ii) the Italian Ministry of Education, University and Research (MIUR): Department of Excellence Program (2018–2022), Department of Biology and Biotechnology "L. Spallanzani", University of Pavia.

Declaration of Competing Interest

The authors declare that they have no known competing financial interests or personal relationships that could have appeared to influence the work reported in this paper.

Acknowledgements

The graphical abstract was created using resources provided by BioRender.com. We gratefully acknowledge Prof. Hirokazu Kawagishi (Shizuoka University, Japan) for generously providing the erinacine and hericenone standard compounds, and Tetrahedron (Paris, France) for kindly donating the ergothioneine standard used in this study.

Appendix A. Supporting information

Supplementary data associated with this article can be found in the online version at doi:10.1016/j.biopha.2025.118204.

Data availability

Data will be made available on request.

References

[1] M.M. Shipley, C.A. Mangold, M.L. Szpara, Differentiation of the SH-SY5Y human neuroblastoma cell line, J. Vis. Exp. (2016) 53193.
[2] L. Agholme, T. Lindström, K. Kågedal, J. Marcusson, M. Hallbeck, An in vitro model for neuroscience: differentiation of sh-sy5y cells into cells with morphological and biochemical characteristics of mature neurons, JAD 20 (2010) 1069–1082.
[3] A. D'Aloia, V. Pastori, S. Blasa, G. Campioni, F. Peri, E. Sacco, et al., A new advanced cellular model of functional cholinergic-like neurons developed by reprogramming the human SH-SY5Y neuroblastoma cell line, Cell Death Discov. 10 (2024) 24.
[4] J.A. Korecka, R.E. Van Kesteren, E. Blaas, S.O. Spitzer, J.H. Kamstra, A.B. Smit, et al., Phenotypic characterization of retinoic acid differentiated SH-SY5Y cells by transcriptional profiling, PLoS ONE 8 (2013) e63862.
[5] T. Coccini, S. Vecchio, M. Crevani, U. De Simone, Cytotoxic effects of 3,4-Catechol-PV (One Major MDPV Metabolite) on human dopaminergic SH-SY5Y cells, Neurotox. Res. 35 (2019) 49–62.
[6] B.J. Goldie, M.M. Barnett, M.J. Cairns, BDNF and the maturation of posttranscriptional regulatory networks in human SH-SY5Y neuroblast differentiation, Front. Cell. Neurosci. 8 (2014) 325.
[7] L. Hromadkova, D. Bezdekova, J. Pala, S. Schedin-Weiss, L.O. Tjernberg, C. Hoschl, et al., Brain-derived neurotrophic factor (BDNF) promotes molecular polarization and differentiation of immature neuroblastoma cells into definitive neurons, Biochim Biophys. Acta Mol. Cell Res. 1867 (2020) 118737.
[8] K. Mori, Y. Obara, M. Hirota, Y. Azumi, S. Kinugasa, S. Inatomi, et al., Nerve growth factor-inducing activity of hericium erinaceus in 1321n1 human astrocytoma cells, Biol. Pharm. Bull. 31 (2008) 1727–1732.
[9] K. Mori, Y. Obara, T. Moriya, S. Inatomi, N. Nakahata, Effects of Hericium erinaceus on amyloid β(25-35) peptide-induced learning and memory deficits in mice, Biomed. Res. 32 (2011) 67–72.
[10] F. Brandalise, V. Cesaroni, A. Gregori, M. Repetti, C. Romano, G. Orrù, et al., Dietary Supplementation of *Hericium erinaceus* increases mossy fiber-CA3 hippocampal neurotransmission and recognition memory in wild-type mice, Evid. Based Complement. Altern. Med. 2017 (2017) e3864340.
[11] P. Rossi, V. Cesaroni, F. Brandalise, A. Occhinegro, D. Ratto, F. Perrucci, et al., Dietary supplementation of lion's mane medicinal mushroom, hericium erinaceus (Agaricomycetes), and spatial memory in wild-type mice, Int. J. Med. Mushrooms 20 (2018) 485–494.
[12] F. Brandalise, E. Roda, D. Ratto, L. Goppa, M.L. Gargano, F. Cirlincione, et al., Hericium erinaceus in neurodegenerative diseases: from bench to bedside and beyond, how far from the shoreline? J. Fungi 9 (2023) 551.
[13] H. Kawagishi, A. Shimada, S. Hosokawa, H. Mori, H. Sakamoto, Y. Ishiguro, et al., Erinacines E, F, and G, stimulators of nerve growth factor (NGF)-synthesis, from the mycelia of *Hericium erinaceum*, Tetrahedron Lett. 37 (1996) 7399–7402.
[14] A. Neuhof, Y. Tian, A. Reska, B.H. Falkenburger, S. Gründer, Large acid-evoked currents, mediated by ASIC1a, accompany differentiation in human dopaminergic neurons, Front Cell Neurosci. 15 (2021) 668008.
[15] D. Scholz, D. Pöltl, A. Genewsky, M. Weng, T. Waldmann, S. Schildknecht, et al., Rapid, complete and large-scale generation of post-mitotic neurons from the human LUHMES cell line, J. Neurochem. 119 (2011) 957–971.
[16] V. Cesaroni, M. Brusoni, C.M. Cusaro, C. Girometta, C. Perini, A.M. Picco, et al., Phylogenetic Comparison between Italian and Worldwide Hericium Species (Agaricomycetes), Int J. Med Mushrooms 21 (2019) 943–954.
[17] E. Roda, E.C. Priori, D. Ratto, F. De Luca, C. Di Iorio, P. Angelone, et al., Neuroprotective Metabolites of Hericium erinaceus promote neuro-healthy aging, Int. J. Mol. Sci. 22 (2021) 6379.
[18] F. Corana, V. Cesaroni, B. Mannucci, R.M. Baiguera, A.M. Picco, E. Savino, et al., Array of metabolites in italian hericium erinaceus mycelium, primordium, and sporophore, Molecules 24 (2019) 3511.
[19] D. Ratto, F. Corana, B. Mannucci, E.C. Priori, F. Cobelli, E. Roda, et al., Hericium erinaceus improves recognition memory and induces hippocampal and cerebellar neurogenesis in frail mice during aging, Nutrients 11 (2019) 715.
[20] W. Krzyczkowski, E. Malinowska, F. Herold, Erinacine A biosynthesis in submerged cultivation of Hericium erinaceum: quantification and improved cultivation, Eng. Life Sci. 10 (2010) 446–457.
[21] D.G. Lee, H.-W. Kang, C.-G. Park, Y.-S. Ahn, Y. Shin, Isolation and identification of phytochemicals and biological activities of *Hericium ernaceus* and their contents in *Hericium* strains using HPLC/UV analysis, J. Ethnopharmacol. 184 (2016) 219–225.
[22] O. Mirante, F. Brandalise, J. Bohacek, I.M. Mansuy, Distinct molecular components for thalamic- and cortical-dependent plasticity in the lateral amygdala, Front Mol. Neurosci. 7 (2014), https://doi.org/10.3389/fnmol.2014.00062.
[23] F. Brandalise, U. Gerber, P. Rossi, Golgi cell-mediated activation of postsynaptic GABAB receptors induces disinhibition of the golgi cell-granule cell synapse in rat cerebellum, PLOS ONE 7 (2012) e43417.
[24] F. Brandalise, B.E. Kalmbach, E.P. Cook, D.H. Brager, Impaired dendritic spike generation in the Fragile X prefrontal cortex is due to loss of dendritic sodium channels, J. Physiol. 601 (2023) 831–845.
[25] D. Ratto, B. Ferrari, E. Roda, F. Brandalise, S. Siciliani, F. De Luca, et al., Squaring the circle: a new study of inward and outward-rectifying potassium currents in U251 GBM cells, Cell Mol. Neurobiol. 40 (2020) 813–828.
[26] F. Giammello, C. Biella, E.C. Priori, M.A.D.S. Filippo, R. Leone, F. D'Ambrosio, et al., Modulating voltage-gated sodium channels to enhance differentiation and sensitize glioblastoma cells to chemotherapy, Cell Commun. Signal 22 (2024) 434.
[27] F. Brandalise, M. Ramieri, E. Pastorelli, E.C. Priori, D. Ratto, M.T. Venuti, et al., Role of Na+ /Ca2+ exchanger (NCX) in glioblastoma cell migration (In Vitro), IJMS 24 (2023) 12673.
[28] F. Brandalise, V. Cesaroni, A. Gregori, M. Repetti, C. Romano, G. Orrù, et al., Dietary supplementation of hericium erinaceus increases mossy fiber-CA3 hippocampal neurotransmission and recognition memory in wild-type mice, Evid. Based Complement Altern. Med 2017 (2017) 3864340.
[29] D. Ratto, B. Ferrari, E. Roda, F. Brandalise, S. Siciliani, F. De Luca, et al., Squaring the circle: a new study of inward and outward-rectifying potassium currents in U251 GBM cells, Cell Mol. Neurobiol. 40 (2020) 813–828.
[30] J. Popko, A. Fernandes, L.M. Lanier, Automated analysis of neuronj tracing data, Cytom. Part A: J. Int. Soc. Anal. Cytol. 75 (2009) 371.
[31] M. Černelič Bizjak, Z. Jenko Pražnikar, S. Kenig, M. Hladnik, D. Bandelj, A. Gregori, et al., Effect of erinacine A-enriched Hericium erinaceus supplementation on cognition: a randomized, double-blind, placebo-controlled pilot study, J. Funct. Foods 115 (2024) 106120.
[32] A.G. Contato, C.A. Conte-Junior, Lion's mane mushroom (Hericium erinaceus): a neuroprotective fungus with antioxidant, anti-inflammatory, and antimicrobial potential—a narrative review, Nutrients 17 (2025) 1307.
[33] I. Szućko-Kociuba, A. Trzeciak-Ryczek, P. Kupnicka, D. Chlubek, Neurotrophic and Neuroprotective Effects of Hericium erinaceus, Int J. Mol. Sci. 24 (2023) 15960.
[34] Y. Qiu, G. Lin, W. Liu, F. Zhang, R.J. Linhardt, X. Wang, et al., Bioactive compounds in *Hericium erinaceus* and their biological properties: a review, Food Sci. Hum. Wellness 13 (2024) 1825–1844.
[35] O.I. Aruoma, J.P.E. Spencer, N. Mahmood, Protection against oxidative damage and cell death by the natural antioxidant ergothioneine, Food Chem. Toxicol. 37 (1999) 1043–1053.
[36] I.K. Cheah, B. Halliwell, Ergothioneine; antioxidant potential, physiological function and role in disease, Biochim. Et. Biophys. Acta BBA Mol. Basis Dis. 1822 (2012) 784–793.

[37] H. Teppola, J.-R. Sarkanen, T.O. Jalonen, M.-L. Linne, Morphological differentiation towards neuronal phenotype of sh-sy5y neuroblastoma cells by estradiol, retinoic acid and cholesterol, Neurochem. Res. 41 (2016) 731–747.
[38] L. Hromadkova, D. Bezdekova, J. Pala, S. Schedin-Weiss, L.O. Tjernberg, C. Hoschl, et al., Brain-derived neurotrophic factor (BDNF) promotes molecular polarization and differentiation of immature neuroblastoma cells into definitive neurons, Biochim. Et. Biophys. Acta BBA Mol. Cell Res. 1867 (2020) 118737.
[39] R. Martínez-Mármol, Y. Chai, J.N. Conroy, Z. Khan, S.-M. Hong, S.B. Kim, et al., Hericerin derivatives activates a pan-neurotrophic pathway in central hippocampal neurons converging to ERK1/2 signaling enhancing spatial memory, J. Neurochem. 165 (2023) 791–808.
[40] H.-T. Huang, C.-H. Ho, H.-Y. Sung, L.-Y. Lee, W.-P. Chen, Y.-W. Chen, et al., Hericium erinaceus mycelium and its small bioactive compounds promote oligodendrocyte maturation with an increase in myelin basic protein, Sci. Rep. 11 (2021) 6551.
[41] S. Mirsadeghi, E. Shahbazi, K. Hemmesi, S. Nemati, H. Baharvand, J. Mirnajafi-Zadeh, et al., Development of membrane ion channels during neural differentiation from human embryonic stem cells, Biochem. Biophys. Res. Commun. 491 (2017) 166–172.
[42] M. Song, O. Mohamad, D. Chen, S.P. Yu, Coordinated development of voltage-gated Na^+ and K^+ currents regulates functional maturation of forebrain neurons derived from human induced pluripotent stem cells, Stem Cells Dev. 22 (2013) 1551–1563.
[43] P. Rossi, E. D'Angelo, J. Magistretti, M. Toselli, V. Taglietti, Age-dependent expression of high-voltage activated calcium currents during cerebellar granule cell development in situ, Pflug. Arch. 429 (1994) 107–116.
[44] F. Brandalise, R. Lujan, R. Leone, F. Lodola, V. Cesaroni, C. Romano, et al., Distinct expression patterns of inwardly rectifying potassium currents in developing cerebellar granule cells of the hemispheres and the vermis, Eur. J. Neurosci. 43 (2016) 1460–1473.
[45] T.A. Zolnik, A. Bronec, A. Ross, M. Staab, R.N.S. Sachdev, Z. Molnár, et al., Layer 6b controls brain state via apical dendrites and the higher-order thalamocortical system, Neuron 112 (2024) 805–820.e4.
[46] S. Soldado-Magraner, F. Brandalise, S. Honnuraiah, M. Pfeiffer, M. Moulinier, U. Gerber, et al., Conditioning by subthreshold synaptic input changes the intrinsic firing pattern of CA3 hippocampal neurons, J. Neurophysiol. 123 (2020) 90–106.
[47] S.K. Panda, G. Sahoo, S.S. Swain, W. Luyten, Anticancer activities of mushrooms: a neglected source for drug discovery, Pharmaceuticals 15 (2022) 176.
[48] P. Ray, S. Kundu, D. Paul, Exploring the therapeutic properties of chinese mushrooms with a focus on their anti-cancer effects: a systemic review, Pharmacol. Res. Mod. Chin. Med. 11 (2024) 100433.
[49] H.-J. Park, Current uses of mushrooms in cancer treatment and their anticancer mechanisms, Int. J. Mol. Sci. 23 (2022) 10502.
[50] P. Nowakowski, R. Markiewicz-Żukowska, J. Bielecka, K. Mielcarek, M. Grabia, K. Socha, Treasures from the forest: Evaluation of mushroom extracts as anti-cancer agents, Biomed. Pharmacother. 143 (2021) 112106.
[51] S.P. Kim, M.Y. Kang, J.H. Kim, S.H. Nam, M. Friedman, Composition and mechanism of antitumor effects of Hericium erinaceus mushroom extracts in tumor-bearing mice, J. Agric. Food Chem. 59 (2011) 9861–9869.
[52] P. Prasher, M. Sharma, A.K. Sharma, J. Sharifi-Rad, D. Calina, C. Hano, et al., Key oncologic pathways inhibited by Erinacine A: a perspective for its development as an anticancer molecule, Biomed. Pharmacother. 160 (2023) 114332.
[53] X. Sheng, J. Yan, Y. Meng, Y. Kang, Z. Han, G. Tai, et al., Immunomodulatory effects of Hericium erinaceus derived polysaccharides are mediated by intestinal immunology, Food Funct. 8 (2017) 1020–1027.
[54] K. Sheng, J. Yang, Y. Xu, X. Kong, J. Wang, Y. Wang, Alleviation effects of grape seed proanthocyanidin extract on inflammation and oxidative stress in a D-galactose-induced aging mouse model by modulating the gut microbiota, Food Funct. 13 (2022) 1348–1359.
[55] S.P. Kim, S.H. Nam, M. Friedman, Hericium erinaceus (Lion's Mane) mushroom extracts inhibit metastasis of cancer cells to the lung in CT-26 colon cancer-tansplanted mice, J. Agric. Food Chem. 61 (2013) 4898–4904.
[56] G. Li, K. Yu, F. Li, K. Xu, J. Li, S. He, et al., Anticancer potential of Hericium erinaceus extracts against human gastrointestinal cancers, J. Ethnopharmacol. 153 (2014) 521–530.
[57] G. Venturella, V. Ferraro, F. Cirlincione, M.L. Gargano, Medicinal mushrooms: bioactive compounds, use, and clinical trials, Int. J. Mol. Sci. 22 (2021) 634.
[58] C.-C. Zhang, X. Yin, C.-Y. Cao, J. Wei, Q. Zhang, J.-M. Gao, Chemical constituents from Hericium erinaceus and their ability to stimulate NGF-mediated neurite outgrowth on PC12 cells, Bioorg. Med Chem. Lett. 25 (2015) 5078–5082.
[59] J. Raman, H. Lakshmanan, P.A. John, C. Zhijian, V. Periasamy, P. David, et al., Neurite outgrowth stimulatory effects of myco synthesized AuNPs from Hericium erinaceus (Bull.: Fr.) Pers. on pheochromocytoma (PC-12) cells, Int. J. Nanomed. 10 (2015) 5853.
[60] K. Mori, S. Inatomi, K. Ouchi, Y. Azumi, T. Tuchida, Improving effects of the mushroom Yamabushitake (Hericium erinaceus) on mild cognitive impairment: a double-blind placebo-controlled clinical trial, Phytother. Res 23 (2009) 367–372.
[61] B.-J. Ma, J.-W. Shen, H.-Y. Yu, Y. Ruan, T.-T. Wu, X. Zhao, Hericenones and erinacines: stimulators of nerve growth factor (NGF) biosynthesis in Hericium erinaceus, Mycology (2010), https://doi.org/10.1080/21501201003735556.